Research on the Design of Variable-Sweep Wing Drive Mechanism for Missiles

Xiaolei Wang[a], Zhiwei Xu[*]

College of Aerospace Engineering, Nanjing University of Aeronautics and Astronautics, Nanjing, China
[a]e-mail: 2940909339@qq.com
[*]Corresponding author's e-mail: zhwxu@nuaa.edu.cn

Abstract. Variable-sweep wings are an important means to meet the flight characteristics of variable geometry missiles. In this paper, a variable-sweep wing structure for missiles was designed. First, a three-dimensional digital model of the wing structure was established. Then, based on the results of computational fluid dynamics simulations, an appropriate actuator was selected. Finally, computational fluid dynamics software was used to study missile models at various sweep angles, comparing and analyzing the aerodynamic characteristics at different speeds. The research summarized the patterns of the lift coefficient, drag coefficient, and lift-to-drag ratio as they change with sweep angle at different Mach numbers.

Keywords: Variable Geometry Structures; Shape Memory Alloy; Aerodynamic characteristics.

1 Introduction

Modern warfare is largely a contest of air power, and air superiority is the foundation and prerequisite for all conventional military operations. Air control is a crucial factor in determining the outcome of a war, and precision strikes are the main forms of combat. Airborne missiles are key weapon systems for gaining air superiority and carrying out precision strikes[1]. The design goal of variable-wing missiles is to resolve the contradictions in the aerodynamic layout design points for different mission types through adaptive changes in the missile's aerodynamic shape. This overcomes the single-function and limited mobility of traditional fixed-wing cruise missiles, aiming to achieve universality for missiles in multiple missions[2].

One of the key technologies for variable-sweep wing aircraft is the design of the variable-sweep drive mechanism. Traditional sweep wing drive mechanisms mainly include hydraulic, crank-rocker, and slider-crank types. Hydraulic mechanisms are not suitable for adaptive aircraft due to their large mass and volume. Crank-rocker mechanisms have the disadvantages of low synchronicity, large errors, and poor stability due to the difficulty in balancing inertia forces and moments, making them unsuitable for

high-speed transmission[3]. Although slider-crank mechanisms have better stability, the complexity of the mechanism is relatively high[4].

This article, based on the three missions of cruise, patrol, and attack carried out by the missile, takes into account the size of the space and control performance to design the deflection structure, and conducts aerodynamic simulation analysis of the missile model under different working conditions.

2 Design of the Missile Wing's Sweep Angle Deflection Structure

2.1 Missile Overall Model Construction

Based on the mission and flight characteristics of the missile, the missile's exterior shape has been designed. The missile model adopts a front-to-back collinear "+"shaped circumferential layout, with a conventional layout along the missile's longitudinal axis. The nose of the missile is designed to be hemispherical, and the wing sections of both the wings and the tail fins are of a double-curved profile. The wings feature a structure with fixed inner wings and variable-sweep outer wings, with the outer wings having a sweep angle range of 30° to 90°. The missile consists of a warhead, body, four wings, and tail fins. The total length of the missile is approximately 1800mm, with a body diameter of 160mm, a wing span of 240mm when fully retracted, an outer wing length of 300mm, and an inner wing height of 16mm. The structural shape and dimensions are shown in Fig.1.

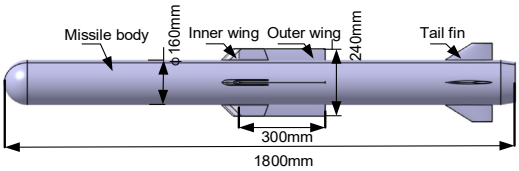

Fig. 1. Missile Exterior and Dimensions with a 90° Wing Sweep Angle.

2.2 Design and Principle Analysis of Wing Sweep Angle Deflection Drive Mechanism

The connection between the flaperon and the missile body is made using a sleeve-type design, with the inner wing fixed to the sleeve. There is a rigid connection between the upper and lower blocks of the sleeve. The overall structural layout is shown in Fig.2.

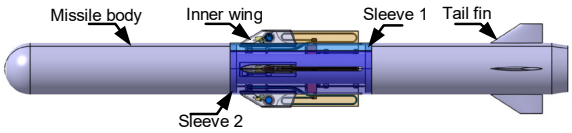

Fig. 2. Schematic Diagram of the Overall Layout of the Wing Structure.

First, the elastic force of the planar spiral spring is used to quickly deflect the flaperon from a sweep angle of 90° to 30°, and then lock it in place. Afterwards, the recovery force of the SMA wire is utilized to drive the flaperon from a sweep angle of 30° to 60°, and lock it again. The structure for the deflection of the flaperon's sweep angle is shown in Fig 3.

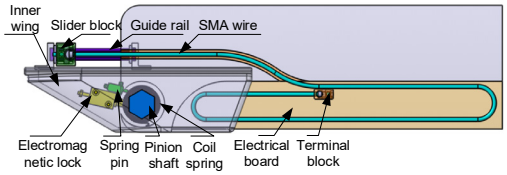

Fig. 3. Schematic Diagram of the Wing Sweep Angle Deflection Structure.

Considering the thin thickness of the wing and the limited arrangement space, this paper designs and uses a non-contact flat spiral spring.

The deformation angle of the springΨ[5]

$$\psi = \frac{12K_1Tl}{Ebh^3} \tag{1}$$

In the formula: K_1 is a coefficient, K_1=1.25, T is the spring torque, l is the spring's unfolded length, E is the modulus of elasticity, b is the spring's width, and h is the spring's thickness. The thickness h of the spring material section.

$$h = \sqrt{\frac{6K_2T}{b[\sigma]}} \tag{2}$$

In the formula: K_2 is a coefficient, K_2 = 2.

The working number of turns n of the spring material.

$$n = \frac{\psi}{2\pi} = \frac{6K_1Tl}{\pi Ebh^3} \tag{3}$$

The working length l of the spring material.

$$l = \frac{Ebh^3\psi}{12K_1T} \tag{4}$$

The pitch t of the spring material.

$$t = \frac{\pi\left(R^2 - R_1^{\,2}\right)}{l} \tag{5}$$

The inner radius R_1 and the outer radius R of the spring.

$$\left.\begin{aligned} R &= \frac{2l}{\psi} - R_1 \\ R &= R_1 + n_0 t \end{aligned}\right\} \tag{6}$$

The strength verification of the spring, σ

$$\sigma = \frac{6K_2T}{bh^2} = \frac{n\pi EhK_2}{K_1 l} \le [\sigma] \tag{7}$$

Based on the aerodynamic load simulation analysis of the wing model obtained in the early stage, the corresponding dimensions of the spiral spring can be calculated.

After the missile maintains a sweep angle of 30° for cruising and patrolling, the wings need to be deflected to a sweep angle of 60° to enter the attack state. The deflection torque of the wings during this process is provided by the Shape Memory Alloy (SMA) wires. The nickel-titanium alloy material, after certain processing, has the shape memory function, which means that after being deformed by an external force in a low-temperature environment, it can return to its initial shape when heated to a certain temperature, hence it is called a shape memory alloy. Inside the SMA material, there are mainly two alloy phases; below the set temperature, it is the martensitic phase, at which time the elastic modulus of the SMA is relatively low, making it prone to deformation; above the set temperature, it is the austenitic phase, at which time the elastic modulus of the SMA is relatively high, and it can generate a large recovery force during deformation, which can be used as an actuator[6].

In order to enable the tensile force generated by the Shape Memory Alloy (SMA) wire to smoothly drive the flaperon to deflect the sweep angle, and to avoid excessive friction resistance between the SMA wire and the outer wing during its operation, the SMA wire should be reasonably arranged. This structure uses an SMA wire with a diameter of 1mm, and the main mechanical properties of the SMA wire are shown in Table 1 as demonstrated by experimental testing. Among them, M_S is the start temperature of the martensitic phase transformation, M_f is the end temperature of the martensitic phase transformation, A_S is the start temperature of the austenitic phase transformation, A_f is the end temperature of the austenitic phase transformation, D_M is the elastic modulus of the martensite, D_A is the elastic modulus of the austenite, ε_l is the maximum residual strain, and the recovery force of the SMA wire is shown in Table 2.

Table 1. Mechanical Properties of 1mm SMA Wire

M_S/°C	M_f/°C	A_S/°C	A_f/°C	D_A/Gpa	D_M/Gpa	ε_l/%
34.2	24.0	40.8	52.3	12.7	43.8	5.2

Table 2. Recovery Force Values of SMA Wire

Pre-stretch amount/%	2	2.5	3	3.5	4	4.5	5	5.5
Resilience force/N	171	191	230	317	390	401	432	470

Based on the aerodynamic field simulation analysis of the wing model from the early stage. The sum of the aerodynamic torque acting on the wing and the recovery torque of the SMA wire is greater than the output torque of the spring at this time, thus the wing can achieve the sweep angle deflection.

2.3 Design of the Wing Sweep Angle Deflection Locking Mechanism

Considering the limited internal space layout due to the relatively small size of the missile's inner and outer wings, an electromagnetic locking device is first used to lock the wing sweep angle when the wing is deflected from 90° to 30°. The electromagnetic locking device is arranged inside the inner wing space, and there is a limiting groove on the inner wing surface that cooperates with the electromagnetic locking device to limit the position of the electromagnetic lock. A schematic diagram of the electromagnetic lock relative to the positioning hole is shown in Fig.4 and Fig. 5.

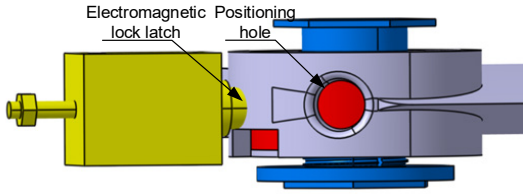

Fig. 4. Schematic Diagram of the Relative Position of the Locking Tongue and Positioning Hole When the Wing Sweep Angle is 90°.

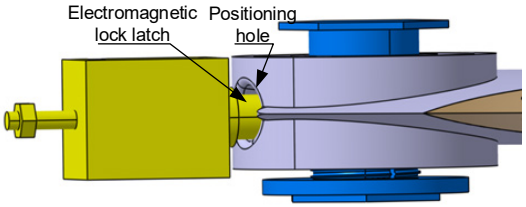

Fig. 5. Schematic Diagram of the Relative Position of the Locking Tongue and Positioning Hole When the Wing Sweep Angle is 30°.

In the mid-section of the spring box sidewall, there is a positioning hole corresponding in size to the spring locking tongue. During the process where the wing sweep angle deflects from 90° to 30°, the spring locking mechanism is in a de-energized state, allowing the tongue to pop out. As the wing deflects around the rotation axis, the tongue is in a compressed state and slides relatively against the sidewall of the spring box. Once the wing sweep angle is deflected to 30°, the tongue pops out to fit with the positioning hole, completing the positioning and locking.

When the flaperon's sweep angle is deflected to 60°, the electromagnetic locking device releases the lock, and this locking task is achieved by a spring pin. The lower end of the side wall of the spring box has a positioning groove corresponding to the

head of the spring pin. When the flaperon is deflected to a sweep angle of 60°, the top of the spring pin comes into contact with the wall of the spring box. At this point, the SMA wire is continuously powered, and the recovery torque of the wire causes the flaperon's sweep angle to deflect in the opposite direction to the one in which the spring pin obstructs the deflection of the sweep angle, thereby achieving the lock. The relevant schematic diagrams are shown in Fig.6 and Fig.7.

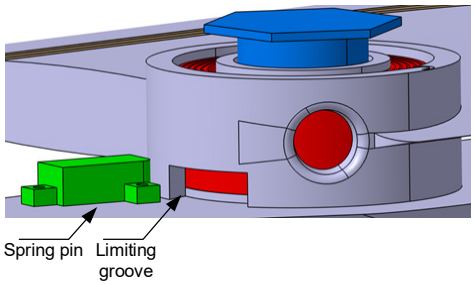

Fig. 6. Schematic Diagram of the Relative Position of the Spring Pin and Spring Box When the Wing Sweep Angle is 90°.

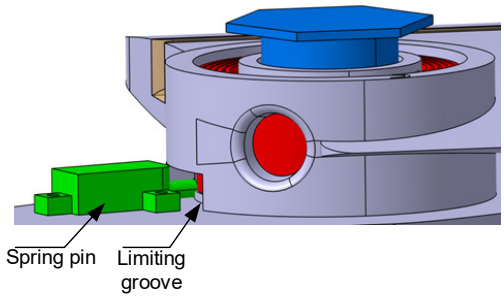

Fig. 7. Schematic Diagram of the Relative Position of the Spring Pin and Spring Box When the Wing Sweep Angle is 60°.

3 Aerodynamic Characteristic Analysis of Variable-Sweep Wing Missiles

To capture the impact of different sweep angle configurations of the air-launched missile on its aerodynamic characteristics, the missile flight angle of attack is set to 5°, and simulations are performed at sweep angles of 30°, 40°, 50°, 60°, 70°, and 80° for missile airspeeds of 0.3Ma, 0.5Ma, 0.9Ma, and 1.1Ma. The material parameters of the fluid are based on the values for an ideal gas. Ultimately, the aerodynamic characteristics of the missile under variable sweep wing conditions are obtained by monitoring the lift and drag coefficients through Fluent monitors[7].

The trend of the lift coefficient change is shown in Fig. 8. Observing the relationship between the lift coefficient and the sweep angle at different airspeeds, it can be seen that at each airspeed, the lift coefficient decreases as the wing sweep angle increases. This is because the local flow velocity on the wing at this time is the component of the actual airspeed along the chord of the wing; the larger the sweep angle, the smaller this component becomes. It is also noted that at the same sweep angle, the lift coefficient tends to increase with increasing airspeed.

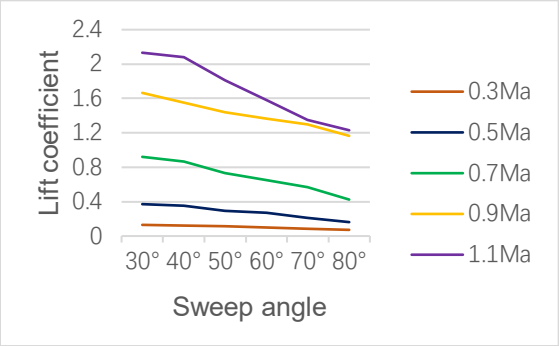

Fig. 8. Schematic Diagram of the Trend of Lift Coefficient Change with Sweep Angle at Different Airspeeds.

The trend of drag coefficient change is shown in Fig.9.From the relationship between the drag coefficient and the sweep angle at different airspeeds, it is known that at low speeds, the main source of missile drag is frictional resistance, which is related to the frontal area. As the sweep angle increases, the frontal area of the missile slowly decreases, and thus the drag also slowly decreases. When the missile's airspeed reaches the transonic range, due to the formation of local shock waves on the wings, the drag on the missile increases dramatically. However, as the sweep angle increases, the occurrence of shock waves is delayed, leading to a corresponding reduction in the drag coefficient, but its value is still greater than that at the same sweep angle at low speeds.

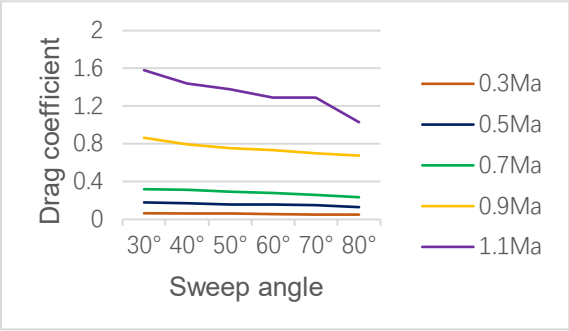

Fig. 9. Schematic Diagram of the Trend of Drag Coefficient Change with Sweep Angle at Different Airspeeds.

The trend of the lift-to-drag ratio change is shown in Fig. 10. The lift-to-drag ratio, defined as the ratio of the lift coefficient to the drag coefficient, is a dimensionless number that describes aerodynamic characteristics. From the relationship between the lift-to-drag ratio and the sweep angle at different airspeeds, it is known that at low speeds, the lift-to-drag ratio decreases as the sweep angle increases. When the airspeed approaches the speed of sound, local shock waves appear on the wings, and the lift-to-drag ratio first increases and then decreases with the increase of the sweep angle. This is due to the increased critical Mach number and the delay of the appearance of shock wave drag caused by the wing sweep. When the sweep angle is too large, the decrease in the lift coefficient exceeds the decrease in the drag coefficient, hence the lift-to-drag ratio decreases with the increase of the sweep angle.

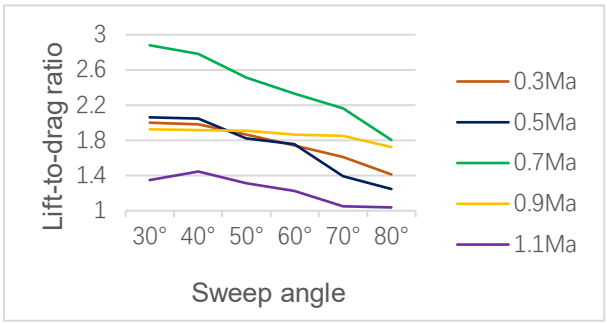

Fig. 10. Schematic Diagram of the Trend of Lift-to-Drag Ratio Change with Sweep Angle at Different Airspeeds.

4 Conclusions

In this paper, based on the flight characteristics of the missile, a variable-sweep wing drive mechanism has been designed, and the following conclusions have been drawn:

Compared to traditional drive mechanisms such as hydraulic systems, the variable-sweep wing drive mechanism designed in this paper is structurally simple and has a small mass and volume. It can effectively achieve the variable-sweep function of the wings while meeting the structural strength requirements.

Through aerodynamic simulation analysis of the missile flow field, it is concluded that the lift coefficient tends to decrease as the wing sweep angle increases. At the same sweep angle, the lift coefficient also increases with the increase of airspeed. When the airspeed approaches the speed of sound, although the drag coefficient and the lift-to-drag ratio may temporarily increase due to the formation of local shock waves on the wings, they generally decrease with the increase of the sweep angle.

References

1. Li Y, Zhang S.J, Zhu YH. Analysis of the Development Trends and Dynamics of Typical Airborne Missiles of the United States and Russia in 2023[J]. Aerospace Defense, 2024, 7(04): 30-37.
2. Liu. X.H, Zhang. S.Z, Miao. H.C, Design and Simulation of Trajectory for Missiles with Variable Wings [J]. Journal of Ballistics, 2020, 40(05): 20-23. DOI: 10.15892/j.cnki.djzdxb.2020.05.005.
3. Cai. Z.J, Gao. Z.C, Design of Variable-Sweep Wing Actuation Mechanism and CFD Simulation [J]. Mechanical Design, 2018, 35(09): 17-22. DOI: 10.13841/j.cnki.jxsj.2018.09.003.
4. Wang. Z.J, A Review of the Current Status of Variable-Sweep Wing Research [J]. China High-Tech, 2019, (05): 31-33. DOI: 10.13535/j.cnki.10-1507/n.2019.05.06.
5. Yang J.R, Ren B.F, Sun S.S. Design and Analysis of the Coil Spring in the Spring Energy Storage Power Generation System[J]. Mechanical Design and Manufacturing, 2021, (09): 145-149. DOI: 10.19356/j.cnki.1001-3997.2021.09.033.
6. Chen J, Li J.Y. Research on the Mechanical Properties of Shape Memory Alloys and Their Application in Morphing Structures[J]. Measurement & Control Technology, 2024, 43(05): 34-41. DOI: 10.19708/j.ckjs.2024.05.003.
7. Gao Y, Li Y.B, Wang Y. Simulation Analysis of the Aerodynamic Characteristics of a Variable Swept Wing Missile[J]. Mechanical Design, 2022, 39(03): 68-73. DOI: 10.13841/j.cnki.jxsj.2022.03.005.